Indian J. Phys. **68A** (1), 1 – 22 (1994)

IJPA
— an international journal

A high energy ion scattering facility for condensed matter physics and materials science studies

K Sekar, G Kuri, P V Satyam, B Sundaravel, D P Mahapatra and B N Dev*
Institute of Physics, Sachivalaya Marg, Bhubaneswar-751 005, Orissa, India

Received 14 September 1993, accepted 8 November 1993

Abstract : A high energy ion scattering experimental facility has been set up in the Ion Beam Laboratory at the Institute of Physics, Bhubaneswar. Some examples of Rutherford backscattering and channeling studies using 1–3 MeV He^+ ions from the recently installed 3MV tandem Pelletron Accelerator are presented. Composition analysis of Cu_3Au and high T_c superconductor material $Bi_2Sr_2Ca_1Cu_2O_8$ and interdiffusion studies at metal-semiconductor interfaces are presented. Planar and axial channeling measurements were made on several systems. For silicon [111] axial channeling the measured critical angle, $\psi_{1/2}$ = 0.85°, and the minimum yield χ_{min} = 0.055 are slightly higher than the theoretical values of 0.65 and 0.03 respectively. Further channeling measurements are presented for a Cu_3Au crystal and an ion beam synthesized three layer epitaxial system Si/$CoSi_2$(680Å)/Si(880Å).

Keywords : Rutherford backscattering spectrometry (RBS), channeling, thin films, Cu_3Au, epitaxial layers, Si/$CoSi_2$/Si, ion beam synthesis

PACS Nos. : 68.35.Bs, 68.35.Fx, 79.20.Rf

Plan of the Article.

1. Introduction

2. High energy ion scattering (HEIS)

2.1. Backscattering spectrometry

2.1.1. Kinematic factor and the energy spectrum

2.1.2. Scattering cross section $\left(\frac{d\sigma}{d\Omega}\right)$ *and the scattering yield*

2.1.3. Stopping cross section (ε)

2.1.4. Energy straggling (Bohr's theory)

2.2. Channeling

* Author for correspondence e-mail: bhupen @ iopb.ernet.in

© 1994 IACS

3. Experimental set-up

4. Experimental examples

4.1. RBS measurements

4.1.1. Bulk crystals

4.1.2. Thin films

4.2. Channeling measurements

4.2.1. Bulk crystals

4.2.2. Epitaxial layers

5. Conclusion

1. Introduction

Nuclear physicists, in their quest for increasingly higher energy ion accelerators, left behind the low energy accelerators, which found tremendous use in materials science and condensed matter physics. In fact, low energy ion accelerators have been specifically designed as tools for experiments in materials science and condensed matter physics. The important role of surface and near-surface regions of materials in modern technology has popularized the low energy ion accelerators, which are useful in analyzing thin layers of materials surfaces. These involve ion-implanted surface and near-surface regions, thin films deposited on materials by various methods, epitaxial layers grown on surfaces of crystalline materials by molecular beam epitaxy and other methods, surface oxidation, catalytic reactions on the surfaces etc. Surface and interface physics, which is a branch of condensed matter physics, has seen phenomenal development in the past decade with two Nobel prizes having been awarded in this field. Low energy ion accelerators (up to a few MeV) have contributed significantly in surface and interface physics.

Depending on the ion energy, ion scattering can be divided more or less into three energy regimes :

- Low Energy Ion Scattering (LEIS) (1 – 20 keV)
- Medium Energy Ion Scattering (MEIS) (20 – 200 keV)
- High Energy Ion Scattering (HEIS) (200 keV – 2 MeV)

Ions of a few keV energy are extremely surface sensitive. Therefore, the LEIS technique is used for the study of the 'first monolayer' (~ 10^{15} atoms/cm^2) of the surface. It has been utilized to determine surface composition and study surface segregation. A review of the LEIS technique and its applications has been published by Aono [1].

Experiments in the MEIS regime use Rutherford backscattering spectrometry and for single crystals, ion channeling and blocking effects as well. Many important problems of surface and interface physics have been solved by the MEIS technique. Surface and interface structure, and surface reconstruction can be determined with high accuracy. Through the detection of the surface disordering, the first convincing experiment on surface melting was performed with the MEIS technique providing the understanding of melting at the

microscopic level [2]. The MEIS technique and its applications have been reviewed by van der Veen [3].

Because of the higher incident energy of the ions in HEIS, the ions can penetrate deeper into the sample and can probe a relatively thick (~ 1 μm) layer. It is ideal for the study of buried interfaces. However, under the channeling condition the technique becomes very much surface sensitive which enables the study of surface composition, reconstruction, relaxation, reaction and phase transition. HEIS has contributed significantly in the determination of crystalline quality of single crystals and epitaxial thin layers, type and density of defects at an interface, impurity lattice location in the bulk crystal and the strain in epitaxial films and superlattice structures.

The ion-channeling is highly sensitive to lattice vibrations and small displacements from regular lattice sites. Therefore the channeling technique is very useful for studying phase transitions (such as Jahn-Teller [4] and charge-density-wave phase transitions [5]) which are accompanied by a structural change. High energy ion channeling studies in high T_c cuprate superconductors across the transition temperature has showed large vibrational changes for the Cu–O rows suggesting that the atoms in these rows become strongly coupled in the superconducting phase [6].

Recently a 3 MV tandem van-de-Graaff (Pelletron) accelerator has been installed in the Institute of Physics, Bhubaneswar and an MeV ion scattering experimental facility has been set up in the Ion Beam Laboratory. In this article we will mainly discuss scattering of ions in the MeV energy regime, that is HEIS, and give some examples of experiments that have been carried out with this set-up.

2. High energy ion scattering (HEIS)

HEIS has several advantages. The ions, due to their higher energy, can penetrate deeper into the sample and thus probe thin films, buried layers and buried interfaces. Charge neutralization of the scattered ions in this energy regime is negligible. The scattered ion yields and energies can be conveniently measured with inexpensive surface barrier detectors. Quantitative estimation of the scattering is rather simple. In this energy regime, the interaction cross sections are sufficiently low so that for the semiconductors and metals the beam induced effects can be neglected or easily corrected for. Reviews and books on the applications of High Energy Ion Scattering are available [7–9]. Here we will present a brief description of the basic aspects of this technique, the experimental set-up at Bhubaneswar and a few experimental examples using this facility.

The typical requirements and characteristics of HEIS experiments are :

- Probe beam — H^+, He^+, other light ions
- Probe beam energy — 1–3 MeV
- Beam diameter — ≈ 0.5–1.5 mm
- Beam current — ≈ 2–20 nA

- Integrated charge on the sample — ≈ 1–40 μC ($6 \times 10^{12} - 2.5 \times 10^{14}$ ions)
- Scattering angle ~ 100–180°
- Energy analyzer — Surface barrier detector; 15–25 keV energy resolution
- Probing depth — ≈ 1–2 µm at normal incidence
- Depth resolution — ≈ 200–300 Å (30–40° Å with tilted targets)
- Mass resolution — Isotopic resolution for target mass upto ≈ 40 amu
- Sensitivity — $10^{-2} - 10^{-4}$ monolayers for heavy surface impurities — $10^{-1} - 10^{-2}$ monolayers for light surface impurities
- Accuracy — 3–5% (typical)

2.1. Backscattering spectrometry :

The basis of MeV ion scattering techniques rests on the fundamental relations that govern ion scattering in solids. The atomic and nuclear collisions can be characterized by the impact parameter of the scattering process. The largest impact parameters possible in a solid are of the order of 1 Å. For such a distant collision, the ions interact primarily through excitation and ionization of valence electrons with energy transfers of the order of 10 eV per collision. These processes have cross sections of the order of atomic dimensions, ~ 10^{-16} cm^2. At smaller impact parameters, the particles make 'harder collisions' causing inner shell excitations and ionizations, for example, excitation of K and L shell electrons, with larger energy transfer and smaller cross section. At the smallest impact parameter, of the order of nuclear dimensions, ~ 10^{-12} cm, the incident ions scatter from the atomic nucleus in a billiard ball type of collision resulting in a large angle scattering with a large energy transfer, ~ 100 keV. The cross sections for these processes are ~ 10^{-24} cm^2. As an energetic ion traverses a solid, it gradually loses its energy by interacting with electrons every monolayer or so, coming to rest tens of micrometers below the surface. A small fraction of the particles undergo energetic nuclear encounters before coming to rest. It is the nuclear backscattering events that constitute the signal in ion scattering studies. The final energy of the particle is determined by the depth at which the scattering event occurred, since the particle loses energy to electrons in penetrating the solid. Electronic encounters are generally called inelastic events while the nuclear backscattering event is usually denoted as an elastic event. The use of ion backscattering as a quantitative materials analysis tool depends on an accurate knowledge of the nuclear and atomic scattering processes.

In Rutherford backscattering spectrometry (RBS) one is concerned with projectiles that move through a target, losing energy along their path, and are scattered by collision with a target atom. The interaction between the projectile and target atom can be described as an elastic collision between two isolated particles and expressed in terms of a *scattering cross section*. The energy of the projectile after the collision can be related to its energy before the collision by means of a *kinematic factor*. As the projectile passes through the scattering medium it suffers an average energy loss dE/dx and this leads to the concept of the *stopping*

cross section. Finally, since there are statistical fluctuations in the energy loss of a projectile as it penetrates a solid, particles entering a solid with a given energy will not have identical energies after travelling the same depth. This phenomenon is called *energy straggling.*

The above four basic physical concepts form the basis of RBS. The kinematic factor K leads to the ability for *mass analysis.* The scattering cross section provides RBS with a *quantitative capability.* The stopping cross section results in the capability for *depth analysis* and energy straggling sets limits on *mass and depth resolution.*

2.1.1. *Kinematic factor and the energy spectrum*

When a particle of mass M_1 moving with constant velocity, collides elastically with a stationary particle of mass M_2, energy will be transferred from the moving to the stationary particle. In backscattering analysis, mass M_1 is that of the projectile atom in the analyzing beam and mass M_2 is that of an atom in the target.

The energy E of the projectile after collision with the target atom, is related to its energy E_0 before the collision by the kinematic factor K defined by

$$E = K\ E_0 \tag{1}$$

where

$$K = \left[\frac{M_1 \cos\theta + \left(M_2^2 - M_1^2 \sin^2\theta\right)^{1/2}}{M_1 + M_2}\right]^2 . \tag{2}$$

The kinematic factor K depends on the masses M_1 and M_2 and the scattering angle θ. If a projectile of known mass M_1 and known energy E_0 is directed at the target of unknown mass M_2, by measuring the energy (E) of particles scattered at an angle θ, the unknown M_2 can be determined.

2.1.2. *Scattering cross section* $\left(\frac{d\sigma}{d\Omega}\right)$ *and the scattering yield*

In backscattering spectrometry particles that are scattered at an angle θ are detected by a solid state detector that subtends a solid angle that is small (typically less than 10^{-2} sr). The number of counts, Y, registered by a detector of 100% efficiency is given by

$$Y = Q\,Nt\,\frac{d\sigma}{d\Omega}\,\Omega \tag{3}$$

where Q is the number of particles that strike the target, N is the volume density of target atoms, t is the target thickness and $\frac{d\sigma}{d\Omega}$ is the average differential scattering cross section for scattering into a solid angle Ω at a scattering angle θ. For small values of Ω the average $<\frac{d\sigma}{d\Omega}>$ can be approximated by the differential scattering cross section $\frac{d\sigma}{d\Omega}$ and this is usually referred to simply as the scattering cross section and is denoted by σ. Thus the yield can be written as

$$Y = \sigma(\theta)\,\Omega\,Q\,Nt. \tag{4}$$

The number of particles incident on the target Q and the number of detected particles Y, can be obtained in an experiment. Then with the knowledge of $\sigma(\theta)$ the number of atoms per unit area of the target *i.e.* Nt can be determined. The differential cross section for an elastic collision between two atoms in which the force of interaction is the Coulomb repulsion of the two nuclei is given by Rutherford's formula, which in the laboratory frame of reference is given by

$$\frac{d\sigma}{d\Omega} = \left(\frac{Z_1 Z_2 e^2}{4E}\right)^2 \frac{4}{\sin^4\theta} \frac{\left\{\left[1 - \left((M_1/M_2)\sin\theta\right)^2\right]^{1/2} + \cos\theta\right\}^2}{\left\{1 - \left((M_1/M_2)\sin\theta\right)^2\right\}^{1/2}} \quad (5)$$

where E is the energy of the projectile immediately before scattering and Z_1 and Z_2 are the atomic numbers of the projectile and the target atom respectively. A beam of 1.0 MeV $^4He^+$ scattering from silicon at $\theta = 170°$ has a cross section $\approx 1.0 \times 10^{-24}\,cm^2\,sr^{-1}$ (*i.e.* 1.0 barn). The same beam scattering from gold has a cross section $\sigma \approx 32.8$ barns. The greater scattering yield from the heavier element is given, approximately by

$$\frac{Y_{Au}}{Y_{Si}} = \left(\frac{Z_{Au}}{Z_{Si}}\right)^2 = (79/14)^2 \approx 32 \quad (6)$$

and illustrates the enhanced sensitivity of RBS to heavy elements. Note also that the cross section for scattering is inversely proportional to the square of the projectile energy. The yield from a 2 MeV $^4He^+$ beam is one-quarter of that for a 1 MeV $^4He^+$ beam.

2.1.3. Stopping cross section (ε)

As an energetic particle passes through a solid it loses energy. For the light particles and for the energies used in RBS the two dominant energy loss processes are :

1. interactions with bound or free electrons in the target *i.e.* electronic stopping (ε_e) and
2. interactions with the screened or unscreened nuclei of the target atoms *i.e.* nuclear stopping (ε_n).

In the total stopping cross section (ε) for beams of $^1H^+$ and $^4He^+$ the nuclear stopping is negligible $(\varepsilon_n \ll \varepsilon_e)$ except at the lowest energies (*i.e.* at the deepest penetration of the probe beam). For example, for 1 MeV He^+ in silicon the rate of energy loss dE/dx, due to the electronic and the nuclear stopping, are 31.7 eV/Å and 0.04 eV/Å, respectively. The rate dE/dx at which a particle loses energy is typically 10–100 eV/Å for $^4He^+$ and dE/dx depends on the energy, E_x, of the projectile. The energy E_x of a particle at a depth x will be given by

$$E_x = E_0 - \int_0^x \frac{dE}{dx}\,dx. \quad (7)$$

The stopping cross section ε is given by

$$\varepsilon = \frac{1}{N}\frac{dE}{dx} \tag{8}$$

ε or dE/dx is a function of projectile energy and their values can be obtained from Ref. [10]. dE/dx for compound targets can also be easily evaluated [11]. With the knowledge of dE/dx, the thickness (Δx) of a thin film sample can be determined from the energy width (ΔE) of the RBS spectrum (see Figure 7).

$$\Delta x = \Delta E/[S_0] \tag{9}$$

where

$$[S_0] = \left[K(dE/dx)_{E_0} + \frac{1}{\cos\theta}(dE/dx)_{KE_0}\right] \tag{10}$$

for normal incidence. The energy loss in the first term is calculated at the incident ion energy E_0 and that in the second term at KE_0. This is called 'surface energy approximation'. The quantity $[S_0]/N = [\varepsilon_0]$ is called the *stopping cross section factor.*

2.1.4. Energy straggling (Bohr's theory)

An energetic particle that moves through a medium loses energy *via* many individual encounters. Such a quantized process is subject to statistical fluctuations. As a result, identical energetic particles, which will have the same initial velocity, do not have exactly the same energy after passing through a thickness of Δx of a homogeneous medium. The energy loss ΔE is subject to fluctuation. This phenomenon is called *energy straggling.* Energy straggling places a finite limit for the precision with which energy losses, and hence depths can be resolved by backscattering spectrometry. Bohr's theory predicts that energy straggling does not depend on the energy of the projectile and that the rms value of the energy variation increases with the square root of the electron density per unit area NZ_2t in the target. For a layer of thickness t, Bohr straggling has a variance

$$\Omega_B^2 = 4\pi \left(Z_1 e^2\right)^2 N Z_2 t. \tag{11}$$

Introducing the concepts discussed in 2.1.1–2.1.4 a schematic Rutherford backscattering spectrum is shown in Figure 1.

2.2. Channeling :

Ion channeling is often used in conjunction with RBS. The channeling phenomenon will be briefly described here. When the incident direction of an ion beam is aligned with a crystallographic axis or plane of a single crystal sample the majority of the ions penetrate (channel) into the crystal. Channeled particles cannot get close enough to the atomic nucleus to undergo large angle Rutherford scattering and hence the backscattering is drastically reduced—in many cases by a factor of about 100. The channeling phenomenon and an

RBS spectrum under channeling condition are schematically shown in Figures 2 and 3 respectively. In fact, the channeling effect is observed within an angular range which depends

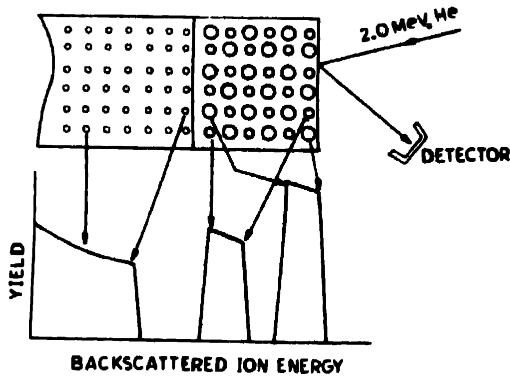

Figure 1. Schematic diagram of a typical backscattering spectrum of a thin film containing two different masses on a low Z elemental substrate.

on the type of ion, the incident energy of the ion, the type of the sample crystal and its specific crystallographic axis or plane along which the beam is incident, and finally on the

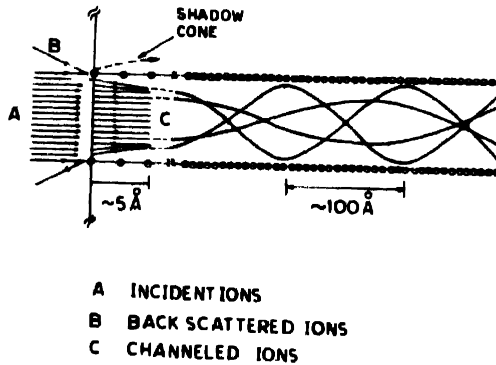

Figure 2. Schematic diagram showing trajectories of particles undergoing scattering at the surface and channeling within the crystal. The shadow cone is also shown in dotted lines.

thermal vibrational amplitude of the constituent atoms in the sample crystal. This angular range is expressed in terms of a *critical angle (or half-angle)* $\psi_{1/2}$, (explained in Figure 11) given by [9]

$$\psi_{1/2} = 0.8\, F_{RS}(\xi)\, \psi_1 \tag{12}$$

where, for axial channeling,

$$\psi_1 = 0.307 \left(\frac{Z_1 Z_2}{Ed}\right)^{1/2} \text{(degrees)} \tag{13}$$

and F_{RS} is the square root of the continuum Moliere potential, evaluated at ξ. E is expressed in MeV. d is the average interatomic distance (in Å) along the channeling axis. When there are

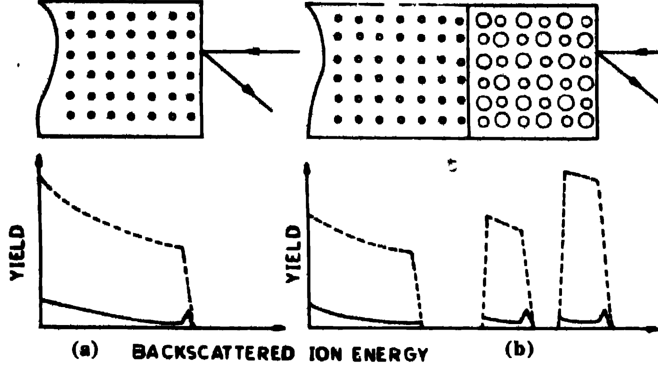

Figure 3. Schematic backscattering spectrum of (a) a monoelemental crystal substrate and (b) a crystalline thin film (compound) on this substrate under channeling (solid lines). The dashed lines show the backscattering spectrum for random incidence.

different types of atoms in a row along the channeling axis, Z_2 is replaced by the average Z_2. $\xi = 1.2\ u_1/a$, where a is the Thomas-Fermi screening radius given by

$$a = \frac{0.4685}{\left(Z_1^{1/2} + Z_2^{1/2}\right)^{2/3}} \tag{14}$$

and u_1 is the one dimensional rms vibrational amplitude.

The ratio of the backscattering yield for the aligned condition to that for the random incidence is denoted by χ_{min} and called the *minimum yield.* It is a measure of the crystalline quality of the sample.

$$\chi_{min} = N_a\, d\pi \left(2u_1^2 + a^2\right) \tag{15}$$

where

N_a is the no. of atoms/Å^3. For a good crystal at room temperature χ_{min} is typically a few percent. This drastic reduction in the backscattering under the channeling condition improves the ion scattering sensitivity to light impurities on the surface.

3. Experimental set-up

A 3 MV tandem Pelletron Accelerator (9SDH2 from NEC) was recently installed at the Institute of Physics, Bhubaneswar. A schematic diagram of the 9SDH2-tandem Pelletron Accelerator and beamlines are shown in Figure 4. Two types of ion sources are present. One (Alphatross) is for providing He and H ions and the other (SNICS) for almost all elements in the periodic table except inert gas ions. A multipurpose scattering chamber (Figure 5), designed to carry out RBS, channeling, Nuclear Reaction Analysis (NRA) and Particle

Induced X-ray Emission (PIXE) studies, is attached to the 45° beam line. A surface barrier detector for the detection of scattered ions, a Si(Li) detector for X-ray detection, a NaI

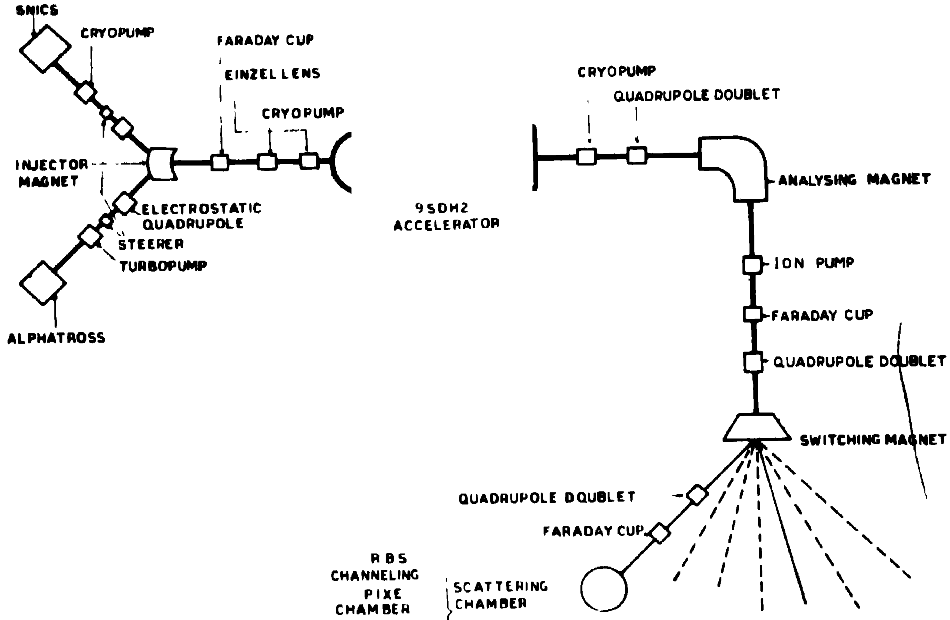

Figure 4. Schematic diagram of the 3 MV 9SDH2-Tandem Pelletron accelerator in the Ion Beam Laboratory at Institute of Physics, Bhubaneswar

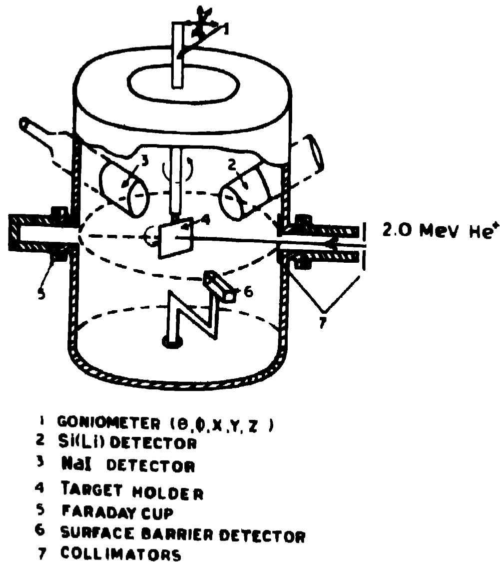

Figure 5. Schematic diagram of the scattering chamber.

detector for detecting γ-rays, a Faraday cup for current integration, and a sample goniometer (x, y, z, θ, ϕ) for channeling experiments are provided through different ports. On the

goniometer the θ rotation has a precision of 0.1° and the ϕ rotation has a precision of 0.3°. The vacuum obtained inside the experimental chamber is in the mid 10^{-7} Torr range. This chamber is coupled to one of the beamlines of the accelerator where better vacuum is maintained. 1–2 MeV He^+ beam is usually used for the RBS and channeling experiments. The beam is collimated by a pair of collimators of dia 1.5 mm separated by a distance of about 1/2 metre. This is done to reduce the divergence of the beam which is essential for the channeling measurements.

The system consists of one surface barrier detector (SBD) which could be set to detect scattered particles over a scattering angle range of 0°–170°. The solid angle subtended by the SBD, Ω, is maintained around 2 msr. The resolution of the SBD is 26 keV and the beam current is in the range of about 5–15 nA. The energy of the incident beam and the scattering angle of the SBD can be varied without disturbing the vacuum system either in the chamber or in the accelerator. This system also has a provision to set an annular SBD to obtain a scattering angle of ≈ 180°. The Si(Li) and the NaI detectors are outside the vacuum. For most of the experiments the goniometer can be taken off and a simple target ladder for loading several samples at a time can be attached to the same port. The goniometer has a combined sample heating and cooling attachment through which the sample temperature can be varied in the 135–1220 K range. The chamber has two viewports and several other ports for various feed throughs. The scattering chamber is provided with a Balzers DIF-set pumping station with a liquid nitrogen trap and a chilled water cooling facility. The scattered particles are detected by an SBD. The detector signal is shaped and amplified and finally with a pulse height analysis the energy spectrum is stored and displayed in a multichannel analyzer (MCA). We use a CANBERA-88 MCA.

4. Experimental examples

In this section RBS measurements on bulk crystals and thin films deposited on crystalline substrates will be given. Section 4.1 will deal with the case of ion beam at random incidence (that is, no channeling). In Section 4.2 we will give examples of channeling measurements.

4.1. RBS measurements :

4.1.1. Bulk crystals

Here we present the composition analysis of a high T_c single crystal material of nominal composition $Bi_2Sr_2CaCu_2O_8$. The backscattering spectrum is shown in Figure 6. The composition can be determined from the heights of the respective edges [11]. We treat this sample to be composed of X_7O_8 molecular units. For normal incidence the signal height at the edge due to the component A in the compound is given by

$$H_A^{\mathrm{Compd}} \quad \left(N_A/N\right) \sigma_A(E_0)\, Q\, \Omega \left(\varepsilon/[\varepsilon_0]_A^{\mathrm{Compd}}\right). \tag{16}$$

Here $\left(N_A/N\right)$ is the number of A atoms in a molecular unit, ε is the energy width corresponding to one channel in the MCA and $\left[\varepsilon_0\right]_A^{\mathrm{Compd}}$ is the stopping cross section factor

of the compound material with scattering from the element A evaluated in the surface energy approximation. On the assumption that $[\varepsilon_0]$ ratios are unity, the spectrum height ratios are

$$\left(H_A/H_{A'}\right) = \left(N_A/N_{A'}\right)\left(\sigma_A/\sigma_{A'}\right) \tag{17}$$

where A and A' are two different elements. For elements with high mass, one can simplify eq. (17) to

$$\left(H_A/H_{A'}\right) = \left(N_A/N_{A'}\right)\left(Z_A^2/Z_{A'}^2\right). \tag{18}$$

The values of $N_A/N_{A'}$ can be obtained from the signal heights in Figure 6. Since the molecular unit being considered is X_7O_8, we get another condition :

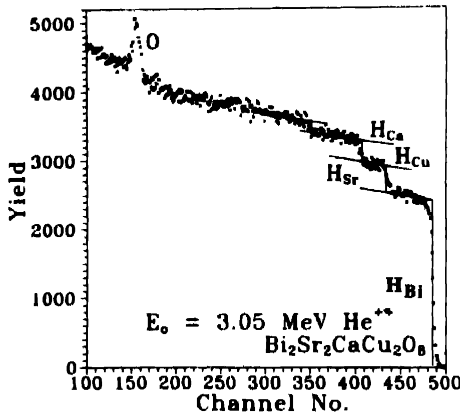

Figure 6. RBS spectrum of a high T_c material of nominal composition $Bi_2Sr_2CaCu_2O_8$. At 3.05 MeV energy of the incident He^{++} ion, oxygen has a resonance non-Rutherford scattering.

$$\left(N_{Bi}/N\right) + \left(N_{Sr}/N\right) + \left(N_{Ca}/N\right) + \left(N_{Cu}/N\right) = 7. \tag{19}$$

From eqs. (18) and (19), we get

$\left(N_{Bi}/N\right) = 2.2$, $\left(N_{Sr}/N\right) = 1.4$, $\left(N_{Ca}/N\right) = 1.1$, $\left(N_{Cu}/N\right) = 2.3$. These values are actually the average values obtained from several RBS spectra measured at different incident ion energies. Therefore, by treating the system as X_7O_8 the determined composition is $Bi_{2.2}Sr_{1.4}Ca_{1.1}Cu_{2.3}O_8$. It should be noted here that the sample could be oxygen deficient. The only cationic part, assuming there are two Bi atoms in the unit, is given by $Bi_2Sr_{1.3}Ca_1Cu_{2.1}$, which indicates Sr-deficiency. We have not attempted to determine the oxygen content of the sample. Usually the edge height for oxygen in the spectrum due to Rutherford scattering would be small. However, with the choice of the incident ion energy an enhanced resonance scattering from oxygen can be obtained as shown in Figure 6. From this enhanced resonance scattering the oxygen content in the material can be determined [12].

4.1.2. *Thin films*

Using the case of thin (~ 1000 Å) film deposited on an Si(111) substrate, we will discuss how RBS measurements are useful in identifying interdiffusion across an interface, determining diffusion coefficients, getting a knowledge of the diffusion barrier at the interface, reaction between the film and the substrate elements, composition of the reacted film etc. We have also developed a simulation program to simulate the spectra for multicomponent multilayer samples. This program has been effectively used to determine the composition of the reacted film, to determine the thickness of very thin films and to determine the extent of surface oxidation. Details of these have been presented in Ref. [13].

Figure 7 shows RBS spectra for an 1160 Å Cu film deposited on a bromine passivated silicon substrate. The film thickness has been determined by quartz crystal thickness monitor during film deposition and later more accurately by RBS simulation [13]. For the as-deposited sample the scattered He^+ from the Cu film appear at higher energies (channel nos. 310–380) while those from the Si substrate below appear at lower energies (channel nos. 50–240). (The quantity of Br is too little to produce any observable feature in

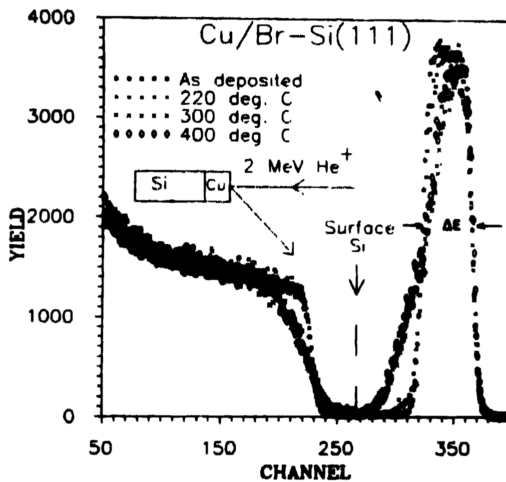

Figure 7. RBS spectra of Cu thin films on bromine-treated Si(111) substrates showing interdiffusion at different temperatures for an annealing time of 30 minutes (From Ref. [13]).

the spectrum [14]). The onset of interdiffusion at the Cu/Si interface at a sample annealing temperature of 220° C is evident from the tailing of Cu part and the high energy edge of the Si part of the spectrum. At higher annealing temperature the extent of interdiffusion is more. From the broadening of the low energy edge of the Cu part, the diffusion coefficient of Cu in Si can be calculated using the procedure given in Ref.[15]. In the present case, for the 300° C-annealed sample, the diffusion coefficient has been found to be ~ 3×10^{-14} cm^2/s .

Figure 8 shows the spectra for a sample where there is a native SiO_2 layer, ~ 20 Å thick, between the Cu film and the Si substrate. In this system, no diffusion is observed for an annealing temperature upto 600° C. This means that the diffusion barrier, in presence of

the thin SiO_2 layer, is much higher. At 700° C annealing the interdiffusion of Cu and Si has occurred. Moreover, Cu and Si reacted to form Cu_3Si compound. This is what happens in

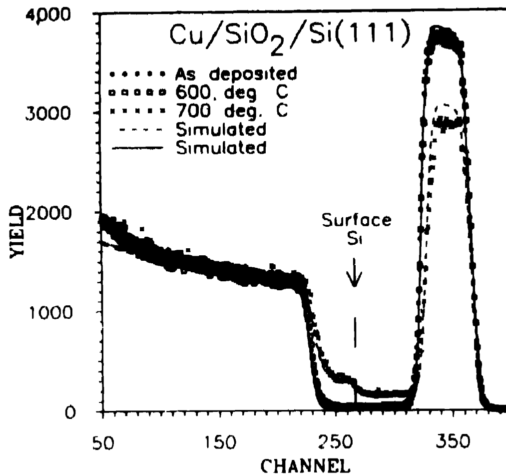

Figure 8. RBS spectra of Cu thin films on native oxide covered Si(111) substrates showing interdiffusion at various temperatures for an annealing time of 30 minutes (From Ref. [13]).

diffusion controlled reactions. The simulated spectra for Cu/Si and Cu_3Si/Si systems show very good agreement with the data. Different cases of simulation are presented in Figure 9. It

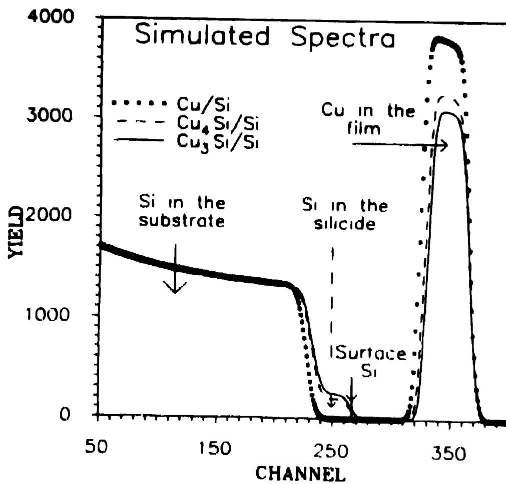

Figure 9. Simulated RBS spectra of Cu/Si, Cu_4Si/Si and Cu_3Si/Si thin film systems. The small step-like feature is due to silicon in the silicide (From Ref. [13]).

is clear that the Cu : Si yield ratios are different for different compounds and hence the compounds can be identified from the yield ratio.

4.2. *Channeling measurements :*

4.2.1. *Bulk crystals*

(a) Si

For demonstration we have taken a (111) oriented silicon wafer (n-type, P doped, $\rho \sim 800$–1500 Ω-cm) for the channeling measurement. The crystal was mounted on the goniometer which allows x, y and z translations and two rotations. One rotation (ϕ) is about an axis perpendicular to the sample surface and the other (θ) is about an axis on the sample surface, the latter being vertical in our case. The θ-rotation is also called tilt angle.

For a given θ (usually a few degrees between the beam direction and surface normal) when the crystal is rotated over a large ϕ, some crystallographic planes are aligned with the beam for specific values of ϕ, where the ions are channeled and the backscattering yield is reduced. Figure 10 shows dips in the scattering yield corresponding to {110} and {112} planar channeling. The yield has been normalized to the yield for random incidence. When the beam is aligned with the [111] crystallographic axis, one observes axial channeling. This is shown in Figure 11, which displays the normalized backscattering yield as a function of tilt

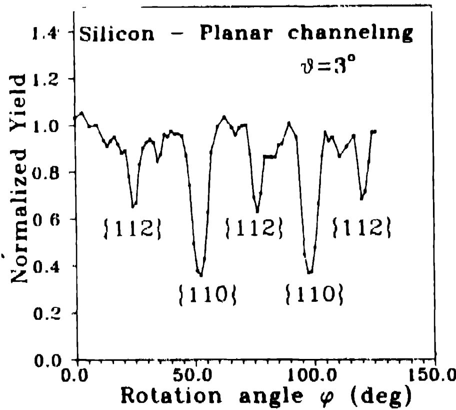

Figure 10. Normalized backscattering yield from a silicon crystal as a function of rotation angle ϕ for a tilt angle $\theta = 3°$ from the [111] crystallographic axis. The dips in the backscattering yield occur when the incident beam is aligned with different crystallographic planes.

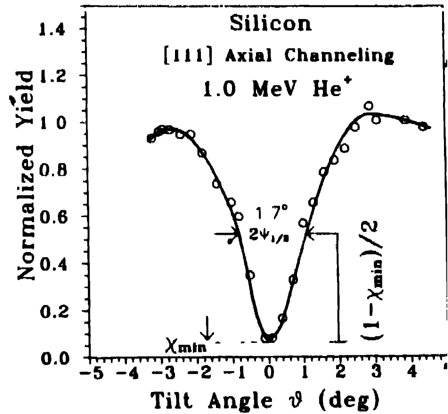

Figure 11. Normalized backscattering yield as a function of the relative angle (θ) between the incident beam direction and the [111] crystallographic axis. The critical angle $\psi_{1/2}$ is shown. Circles denote experimental points and the solid line is to guide the eye.

angle θ. Perfect alignment of the [111] crystallographic axis with the incident He$^+$ beam direction corresponds to $\theta = 0$ and gives rise to the dip. The backscattering spectrum, obtained in the [111] axial channeling condition, is shown in Figure 12 marked 'aligned'. The spectrum obtained for random incidence, that is when the beam is neither aligned to an axis nor to a plane, is also shown in Figure 12 marked 'random'. The peak around channel no. 230 is called surface peak. This peak basically arises from scattering from the topmost atomic layer of the surface. It is only the atoms below the surface which are shadowed and are unable to contribute significantly to the backscattering.

The small feature around channel no. 170 is due to oxygen present in a thin oxide layer on the surface. The peak around channel no. 130 is due to carbon. Part of the carbon was present when the sample was inserted into the scattering chamber. The rest is from adsorption of hydrocarbons on the surface, which comes from the oil used in the diffusion pump. The small features are more prominent on the 'aligned' spectrum because they ride on a low background. This is why the RBS technique under channeling condition become extremely surface sensitive. This feature makes quantitative determination of surface impurities in the monolayer (~ 10^{15} atoms/cm^2) and submonolayer levels possible. From the surface peak intensity it is possible to determine surface atomic structure, which usually involves reconstruction and relaxation [16]. This aspect is beyond the scope of this article. However, the interested reader may refer to the review articles [7,8] and books [9].

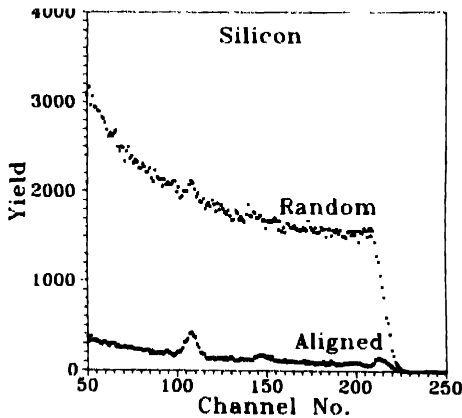

Figure 12. Backscattering spectra for the Si sample taken at the channeling condition ('aligned') and at random incidence ('random'). The yield ratio χ_{min}, taken below the surface peak, is 0.055.

The scattering yield ratio taken in a window behind the surface peak for the aligned and random conditions is denoted by a parameter χ_{min}, called the minimum yield. The value of χ_{min} represents the crystalline quality of the sample. Obviously a small value of the minimum yield signifies better channeling, and hence better quality of the crystal. Our measured value is χ_{min} = 0.055, *i.e.*, 5.5%, which agrees well with the value of 0.03 measured by Picraux *et al* [17] with much smaller beam divergence and better precision in tilt angle. The theoretical value of χ_{min} for [111] axial channeling in a perfect silicon single crystal at room temperature, obtained from eq. (15), is 0.03.

Our measured critical angle $\psi_{1/2}$, as shown in Figure 11, is 0.85°. This is slightly larger than that (0.69°) measured by Picraux *et al.* The theoretical value obtained from eqs. (12), (13) and (14) is 0.65°.

(b) Cu_3Au

To our knowledge channeling measurements have not been made so far on Cu_3Au crystals. Cu_3Au is an interesting system. It undergoes an order-disorder transition at 390° C which

can be studied by channeling. Our goniometer has the provision of heating the sample upto 950° C. Moreover, Cu_3Au crystals show surface reconstruction [18], which also can be studied by channeling. However, the study of surface reconstruction would require an atomically clean surface, which can only be prepared and maintained in ultrahigh vacuum (UHV, pressure $\leq 10^{-10}$ Torr) environment. This is our next step to set up an RBS and channeling experimental facility under UHV condition.

Here we briefly present the results of the measurements on a [110] oriented Cu_3Au crystal. Details will be presented elsewhere. Figure 13 shows the planar channeling results. As the sample is rotated through ϕ the ion beam channels through different sets of planes giving rise to the dips in the backscattering spectrum. The backscattering spectrum for the random incidence and for the [110] axial channeling are shown in Figure 14. The minimum yield χ_{min} is 0.25. The theoretical value of χ_{min} at room temperature estimated from the

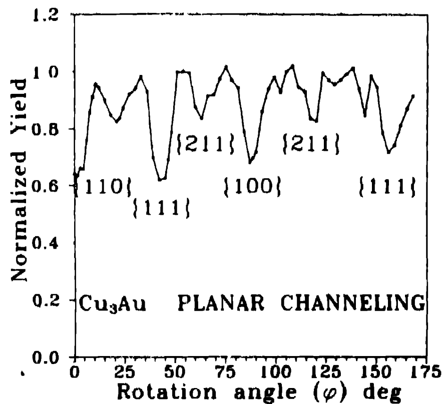

Figure 13. Backscattering yield as a function of rotation angle (ϕ) for a Cu_3Au crystal. The planar minima are seen as dips.

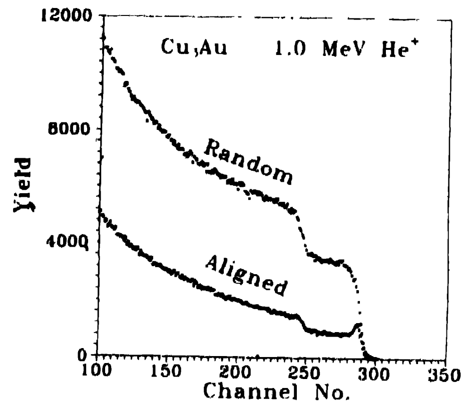

Figure 14. Backscattering spectra for the Cu_3Au sample taken at the random condition and under [110] axial channeling condition. χ_{min}, measured below the Au surface peak, is 0.25.

continuum model is 0.02. It should be pointed out that surface contamination, lattice defects, mosaicity etc., always tend to increase the observed value of χ_{min}. Picraux *et al* [17] observed a $\chi_{min} = 0.08$ for [110] axial channeling in GaSb, for which the predicted value is 0.02.

Figure 15 shows the Au backscattering yield as a function of tilt angle (θ) for the [1$\bar{1}$0] axial channeling. The measured value of the critical angle $\psi_{1/2}$ is 1.45° compared to the theoretical estimate of 1.29°.

The actual composition of Cu_3Au may vary slightly around the ideal value [18]. From the heights H_{Au} and H_{Cu} on the random backscattering spectrum and eq. (17), we have determined the composition to be $Cu_{0.78}Au_{0.22}$.

4.2.2. *Epitaxial layers*

The growth of an oriented single crystal film upon a single crystal substrate of another is called epitaxial growth and the oriented film is called an 'epitaxial layer' or 'epilayer'. Epitaxy

has become increasingly important for advanced electronic and optoelectronic applications. These include high speed three dimensional devices, integrated waveguides, hybrid applications, multilayer and quantum well structures. Depending on the applications the layer thickness vary from a few to several thousand monolayers. The electronic properties of epitaxial thin films and superlattices are intimately dependent on the atomic composition, structure and abruptness of the interface as well as the crystalline perfection, defect distribution and strain in the film.

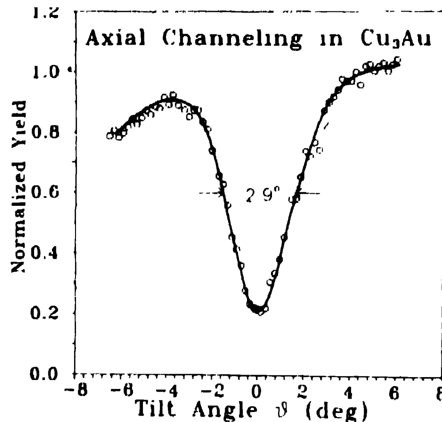

Figure 15. Backscattering yield for [110] axial channeling from the Cu_3Au crystal as a function of tilt angle θ.

It will be useful to explain some aspects of epitaxy here. In heteroepitaxy the film material is different from that of the substrate. This involves lattice mismatch. Let us take the example of a $CoSi_2$ film on a Si substrate. $CoSi_2$ has cubic CaF_2 structure with bulk lattice parameter 1.2% smaller than that of Si. For a pseudomorphic growth, *i.e.* atomic rows in the overlayer being commensurate with substrate atomic rows (Figure 16(a)), the $CoSi_2$ lattice expands in the directions parallel to the surface and contracts in the direction normal to the surface. Therefore, the $CoSi_2$ film is under tensile strain parallel to the interface and under compressive strain perpendicular to it. Strained layer systems have many interesting properties [19] involving modifications of electronic band structures and the promise for band gap engineering to fabricate new materials.

As the film thickness increases the film cannot sustain the strain and tend to relax to its own lattice parameter by introducing dislocations. A completely relaxed situation is schematically shown in Figure 16(b). Between the two extremes shown in Figure 16(a) and 16(b) there could be also partially relaxed films.

With the RBS and channeling techniques it is possible to measure the strain in the film and the dislocation density at the interface. Also from off-normal axial channeling measurements it is possible to determine the stacking fault at the interface [9,20,21].

For growing epilayers, techniques like Metal Organic Chemical Vapour Deposition (MOCVD), Molecular Beam Epitaxy (MBE), Reactive Deposition Epitaxy (RDE), Solid

Phase Epitaxy (SPE) etc. are usually used. However, it has been recently recognized that Ion Beam Synthesis (IBS) is a very useful technique to grow buried, and probably better, epilayers. In the IBS technique, low energy ions of one element is implanted into a substrate. A reaction between the implanted species and the host atoms is caused by annealing, which

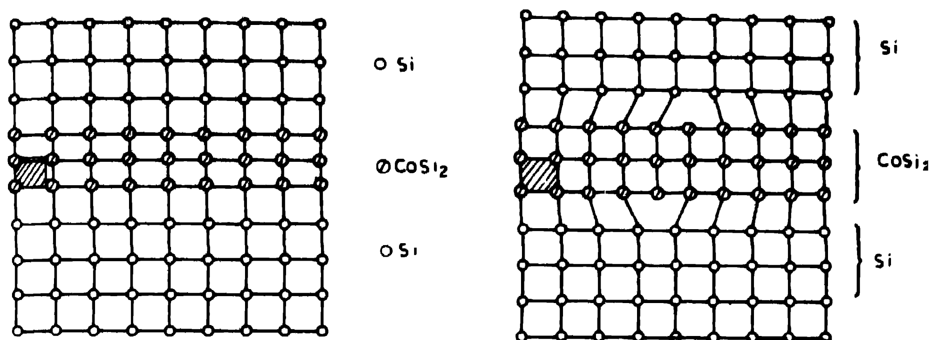

Figure 16. Schematic description of an epitaxial multilayer, (a) the pseudomorphic growth with the overlayer ($CoSi_2$) under strain, (b) strain is relieved by interface misfit dislocations. The hatched square shows the free $CoSi_2$ unit cell.

produces a buried epilayer of the desired compound. It has been shown that a buried $CoSi_2$ epilayer in Si has better transport properties than the epilayers grown on silicon single-crystal surfaces by other conventional methods. In fact, IBS is the only technique which has enabled the fabrication of device quality Si/$CoSi_2$/Si heterostructures on device compatible Si(100) [22].

In this section, we present RBS and channeling measurements on an IBS-prepared buried $CoSi_2$ epilayer. This sample will be denoted by Si/$CoSi_2$/Si. The backscattering spectrum for the random incidence is shown in Figure 17. The thickness of the $CoSi_2$ layer and that of the top Si layer have been determined from simulation (not shown here) to be 680 Å and 880 Å respectively.

From the figure one can notice the clear reduction in the aligned backscattering yield. The part of the spectrum appearing at the higher channel no. (around channel no. 220–260) is due to Co in the $CoSi_2$ layer. The part of the spectrum from around channel no. 190–210 is the contribution from the top Si layer. From around channel no. 160–180 is the contribution of Si from the $CoSi_2$ layer. The signal from the lower channels is from the Si substrate itself.

From the aligned spectrum and the random spectrum χ_{min} calculated from the Si signal of the top Si layer is 7.3% and from the Co signal the χ_{min} is 7.1% and from the substrate Si it is around 20%. From the χ_{min} value one can tell about the crystallinity of the layer under study. From the χ_{min} value obtained from the top Si layer and the $CoSi_2$ layer it is clear that the $CoSi_2$ layer is in good alignment with the top Si layer. But if one compares the χ_{min} value obtained from the substrate (20%) and the $CoSi_2$ layer (7.1%) it is clear that there are defects at the interface between the $CoSi_2$ layer and the bulk Si substrate.

The backscattering yield from the $CoSi_2$ layer as a function of tilt angle (θ) for the [111] axial channeling is shown in Figure 18. The measured value of $\psi_{1/2} = 0.85°$ compares well with theoretical value of 0.87° expected for a $CoSi_2$ crystal.

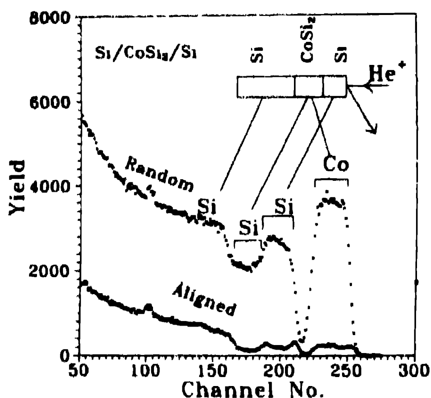

Figure 17. Backscattering spectra for the $Si/CoSi_2$(680 Å)/Si(880 Å) sample taken under [111] axial channeling condition and at random incidence. χ_{min}, measured in the Co region, is 0.071 or 7.1%, which indicates good crystalline quality of the $CoSi_2$ layer.

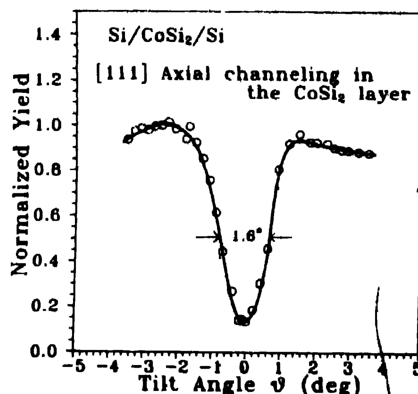

Figure 18. Backscattering yield from the $CoSi_2$ layer of the epitaxial trilayer system $Si/CoSi_2/Si$ as a function of tilt angle θ.

As shown in Figure 16, in heteroepitaxial pseudomorphic growth the epilayer is strained. The amount of strain can be determined from off-normal axial channeling measurements [20]. We have not made these measurements for the $Si/CoSi_2/Si$ sample yet. However, for this sample we have already determined the strain and interface bonding geometry using X-ray diffraction and X-ray standing wave techniques [23]. In many cases the epilayer relaxes by introducing dislocations, which relieve strain [Figure 16(b)]. Dislocations or any other form of defects at the interface can be identified from the ion energy dependence of the interface peak intensity in the aligned spectrum and the defect density can be determined [21].

Now that there are several MBE facilities available in the country for growing epitaxial films, the RBS and channeling techniques will provide a very important tool for characterizing these epilayers.

5. Conclusion

An RBS and channeling experimental facility has been set up in the Ion Beam Laboratory of the Institute of Physics, Bhubaneswar. The experiments are performed using MeV ion beams from the recently installed 3 MV tandem Pelletron accelerator. Various experiments have been performed so far. Here we have presented some examples, where ~ 1–3 MeV He^+ or He^{++} ions have been used. Examples have been given for the determination of thickness and composition of thin films, composition of bulk crystals, studies of interdiffusion at an interface, reaction in thin films etc. using the RBS technique. Channeling measurements

were made on single crystals of silicon and Cu_3Au, and an epitaxial three-layer system $Si/CoSi_2(680\ Å)/Si(880\ Å)$. The crystallinity or quality of the single crystal and epilayers are determined from the value of minimum yield, χ_{min}. At present the experiments are carried out under high vacuum condition ($10^{-6} - 10^{-7}$ Torr). In the near future, we plan to carry out these experiments under ultra-high vacuum ($\leq 10^{-10}$ Torr) condition which will enable us to study atomically clean surfaces.

Acknowledgments

We are thankful to Dr. S Mantl for providing the $Si/CoSi_2/Si$ sample and Dr. P Sen for the Cu_3Au sample. The BiSrCaCuO sample was from Mr. S K Bandyopadhyay. We acknowledge the help given by the accelerator operators and the technical staff and Mr. Ramakanta Nayak for drawing many figures. Finally, we would like to thank Prof. V S Ramamurthy for encouragement in these activities.

References

[1] M Aono 1984 *Nucl. Instrum. Meth.* **B2** 374

[2] J W M Frenken and J F van der Veen 1985 *Phys. Rev. Lett.* **54** 134

[3] J F van der Veen 1985 *Surf. Sci. Rep.* **5** 199

[4] T Haga, K Shimuzu, Y Abe and Y Kino 1981 *Solid State Commun.* **38** 187

[5] T Haga, Y Abe and Y Okwamoto 1938 *Phys. Rev. Lett.* **51** 678

[6] R P Sharma, L E Rehn, P M Baldo and J Z Liu 1989 *Phys. Rev. Lett.* **62** 2869

[7] L C Feldman 1989 *CRC Crit. Rev.* **10** 143

[8] W M Gibson and Shin Hashimoto *Preprint* (State University of New York at Albany, New York)

[9] L C Feldman, J W Mayer and S T Picraux 1982 *Materials Analysis by Ion Channeling* (New York : Academic)

[10] J F Ziegler and W K Chu 1974 *At. Data Nucl. Data Tables* **13** 483

[11] W K Chu, J W Mayer and M A Nicolet 1978 *Backscattering Spectrometry* (New York : Academic)

[12] J Li, L J Matienzo, P Revesz, Gy Vizkelethy, S Q Wang, J J Kaufman and J W Mayer 1990 *Nucl. Instrum. Meth.* **B46** 287; J Li, J W Mayer and E G Colgan 1991 *J. Appl. Phys.* **70** 2820

[13] K Sekar, P V Satyam, G Kuri, D P Mahapatra and B N Dev 1993 *Nucl. Instrum. Meth.* **B73** 63

[14] On a Si(111) surface there are 7.8×10^{14} surface Si atoms per cm^2 in one atomic layer. This is called a 'monolayer'. Thus in general a monolayer is $\approx 10^{15}$ atoms/cm^2. The quantity of adsorbed Br on the Si(111) surface is less than 1/2 monolayer, *i.e.*, $< 4 \times 10^{14}$ atoms/cm^2. Bromine adsorption was used to passivate dangling bonds on the Si surface. It inhibits the oxide growth [K Sekar, P V Satyam, G Kuri, D P Mahapatra and B N Dev 1992 *Nucl. Instrum. Meth.* **B71** 308]

[15] S M Myers and R A Langley 1975 *J. Appl. Phys.* **46** 1034; P M Hall and J M Morabito 1976 *Surf. Sci.* **54** 79; S K Sharma, S Banerjee, Kuldeep and Animesh K Jain 1990 *Appl. Phys.* **A50** 365

[16] M Prutton 1983 *Surface Physics* (Oxford : Oxford University Press)

[17] S T Picraux, J A Davies, L Eriksson, N G E Johansson and J W Mayer 1969 *Phys. Rev.* **B180** 873

[18] See for example, Y Huang and J M Cowley 1993 *Surf. Sci.* **289** 340

[19] T P Pearsal 1989 *CRC Critical Reviews in Solid State and Materials Science* **15** 551

[20] Shin Hashimoto, J L Peng, W M Gibson, L J Schowalter and R W Fathauer 1985 *Appl. Phys. Lett.* **47** 1071 ; Shin Hashimoto, Y Q Feng, W M Gibson, L J Schowalter and B D Hunt 1986 *Nucl. Instrum. Meth.* **B13** 45

[21] Shin Hashimoto, L S Wielunski, J L Peng, W M Gibson and L J Schowalter 1986 *Nucl. Instrum. Meth.* **B13** 65

[22] A E White, K T Short, R C Dynes, J P Garno and J M Gibson 1987 *Appl. Phys. Lett.* **50** 95 ; Alice E White, K T Short, Karen Maex, R Hull, Yong-Fen Hsieh, S A Audet, K W Goossen, D C Jacobson and J M Poate 1991 *Nucl. Instrum. Meth.* **B59/60** 693

[23] P V Satyam and B N Dev 1994 *Indian J. Phys.* **68A** 23 ; P V Satyam, B N Dev, T Gog, G Materlik, R Jebasinki and S Mantl *Preprint* **IP/BBSR/93-35**